On the relation between asymmetries in the ring current and magnetopause current

S. Haaland[1,2] and J. Gjerloev[3,2]

Received 19 August 2013; revised 17 October 2013; accepted 13 November 2013; published 6 December 2013.

[1] Motion of charged particles in the Earth's magnetosphere sets up a system of currents. Current continuity requires that these currents are closed, either locally or via other current systems. In this paper, we have investigated whether magnetopause surface currents can contribute to ring current closure. Using measurements from the Cluster constellation of spacecraft, we calculated thickness and current density of the magnetopause current layer for a large number of flank magnetopause traversals. For each event, we consulted sectorial ring current indices, derived from SuperMAG—a large constellation of ground-based magnetometer stations. SuperMAG results show a significant and persistent dawn-dusk asymmetry in ground magnetic perturbations which indicates a more intense ring current on the duskside. The asymmetries become more pronounced during disturbed magnetospheric conditions, indicating an increased divergence of the current and closure through other current systems. A similar response to geomagnetic activity is also observed at the magnetopause. Duskside magnetopause current densities are generally higher than their dawnside counterparts, and also, the magnetopause asymmetry becomes more pronounced during disturbed conditions. Although the two current systems are related to different processes—gradient drift of energetic plasma sheet particles for the ring current and a surface current due to differential motion of ions and electrons inside the magnetopause interface for the magnetopause current—the results demonstrate a mutual relation between the two current systems.

Citation: Haaland, S., and J. Gjerloev (2013), On the relation between asymmetries in the ring current and magnetopause current, *J. Geophys. Res. Space Physics*, *118*, 7593–7604, doi:10.1002/2013JA019345.

1. Introduction

[2] Motion of charged particles in the Earth's magnetosphere sets up a number of current systems. In this paper, we investigate the relation between two of the most pronounced of these current systems: the ring current and the magnetopause current.

[3] The ring current is caused by differential motion of energetic ions and electrons around the Earth as a result of gradients in the dipolar-like magnetic field. The presence of terrestrial ring current was postulated already by *Størmer* [1912] [see also *Egeland and Burke*, 2012], but the first unambiguous observations followed almost 50 years later from Explorer IV magnetometer observations [*Smith et al.*, 1960]. To the first order, the ring current is often assumed to be symmetric, i.e., it forms a closed circular loop around the Earth with its peak current density around 3–5 Earth radii (R_E) distance and a total magnitude of the order of 10^6 A. The strength of the ring current varies with geomagnetic conditions and is strongly influenced by geomagnetic storms [e.g., *Akasofu and Chapman*, 1961], though.

[4] Hints of an azimuthally asymmetric ring current were suggested in the late 1960s [e.g., *Akasofu and Chapman*, 1964; *Cummings*, 1966], and the first observations of the asymmetry were made in the early 1970s [e.g., *Frank*, 1970; *Langel and Sweeney*, 1971]. Asymmetries were mainly attributed to either field-aligned currents [*Fukushima and Kamide*, 1973] or cross-tail currents [e.g., *Akasofu*, 1980]. It was also noted that asymmetries tended to become larger during storm time conditions [e.g., *Liemohn et al.*, 2001; *Weygand and McPherron*, 2006]. As more in situ observations became available, it also became clear that the ring current has a radial profile, with a weaker inner ($\simeq 3\ R_E$) component flowing eastward and a stronger outer ($\simeq$ 5–7 R_E) component flowing westward [*Le et al.*, 2004; *Jorgensen et al.*, 2004; *Liu et al.*, 2006].

[5] Changes in ring current intensity cause magnetic perturbations that can be measured with ground-based instrumentation. The published disturbed storm time (*Dst*) and symmetry (SYM-H) indices are designed to measure the intensity of the ring current. These indices make use of

[1]Max-Planck Institute for Solar Systems Research, Katlenburg-Lindau, Germany.
[2]Birkeland Centre for Space Science, University of Bergen, Bergen, Norway.
[3]Applied Physics Laboratory, Johns Hopkins University, Laurel, Maryland, USA.

Corresponding author: S. Haaland, Max-Planck Institute for Solar Systems Research, Katlenburg-Lindau DE-37191, Germany. (Stein.Haaland@issi.unibe.ch)

2169-9380/13/10.1002/2013JA019345

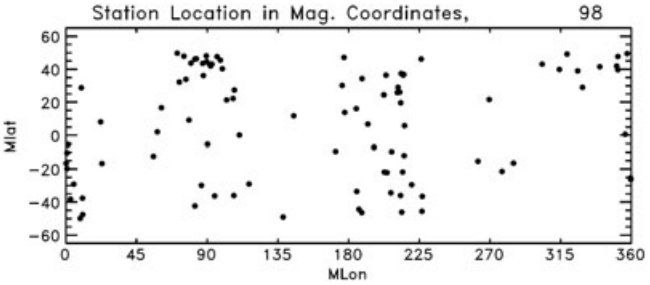

Figure 1. Map of SuperMAG stations used to derive sectorial ring current indices. In total 98 stations within ±50° magnetic latitude contribute to the sectorial ring current indices.

four or six geomagnetic observatories near Earth's magnetic equator and only provide a measure of the symmetric part of the ring current.

[6] Using an extensive set of stations in the SuperMAG collaboration, *Newell and Gjerloev* [2012] introduced a new set of partial ring current indices, which provide separate estimations of the dusk, midnight, dawn, and noon sector parts of the ring current, respectively. Their study also revealed consistent asymmetries in the behavior of the ring current, with a faster and stronger enhancement of the dusk-side part of the ring current as a response to storms and substorms. This asymmetry naturally raises the question about current closure.

[7] *Newell and Gjerloev* [2012] suggested that closure via the ionosphere through field-aligned currents was needed to preserve current continuity. Most of the earlier studies of the asymmetric ring current also suggested that the diverging parts of the ring current are closed through field-aligned currents into the ionosphere [e.g., *Crooker*, 1972; *Crooker and McPherron*, 1972; *Fukushima and Kamide*, 1973] or partly by cross-tail currents. Likewise, noon-midnight asymmetries were explained by an additional nightside cross-tail current [e.g., *Kawasaki and Akasofu*, 1971; *Iijima et al.*, 1990, and references therein], which to some extent is reflected in the ASYM-H index.

[8] The present study was motivated by the question of dawn-dusk asymmetry and current closure of the ring current. The initial idea was to utilize recent advantages in methodology and the large number of magnetopause crossings from the Cluster mission to investigate the role of the magnetopause for ring current closure.

[9] Magnetopause currents (sometimes termed Chapman-Ferraro currents; after *Chapman and Ferraro* [1930]) are primarily set up by differential motion of ions and electrons inside the magnetopause interface. When solar wind particles encounter the gradient caused by the geomagnetic field, around 10–12 R_E upstream, ions and electrons are deflected in different directions as a result of the Lorentz force. This motion creates an electric current directed eastward in the equatorial plane. Ions and electrons from the magnetospheric side also contribute to the current. Typical current densities are of the order of 10–100 nA/m^2. Closure of the magnetopause currents is mainly thought to take place trough the cross-tail currents or through other parts of the magnetopause.

[10] Since magnetopause currents are much weaker than the ring current and the radial distance from the Earth much larger, their ground magnetic perturbations are very much smaller and difficult to distinguish from the much larger perturbations caused by other current systems. Information about magnetopause current density, current directions, and total current intensity as well as possible large-scale asymmetries therefore needs to be based on in situ observations.

[11] Whereas key magnetopause parameters such as thickness, orientation, and current density have been investigated in a number of studies (see e.g., *Hasegawa* [2012], for a comprehensive overview) since the first magnetopause observations in the early 1960s [*Cahill and Amazeen*, 1963], reports about persistent dawn-dusk asymmetries are rare.

[12] In this study, we investigate the mutual influence between dawn-dusk asymmetries in the ring current and magnetopause currents. In particular, we investigate whether magnetopause currents can provide parts of the required ring current closure. The rationale is that changes in the Earth's magnetic field configuration can alter the drift patterns of the particles forming the ring current and sometimes cause loss of drifting particles through the dayside magnetopause.

[13] To address this issue, we have collected a large number of observations from the dawn and dusk flanks of the Earth's magnetopause. From these observations, we then calculated the local current density and also the total current where possible. We thereafter tried to find any statistical correlations between the ring current and magnetopause currents. In particular, we investigate whether the response to geomagnetic activity shows a similar behavior in the two current systems.

[14] The paper is organized as follows: In section 2, we present the data basis for this study, including existing experimental evidence for an asymmetric ring current. This is largely based on the recent findings by *Newell and Gjerloev* [2012] where a large array of ground-based magnetic perturbations was used to study the ring current behavior. The methodology to estimate magnetopause currents is outlined in section 3, followed by a description of the data sets and an assessment of their quality in section 4. Results are given in section 5 and discussion of these in section 6. Section 7 summarizes the paper.

2. Data and Instrumentation

[15] The data basis for this study is the extensive set of ground magnetometer observations from the SuperMAG collaboration [*Gjerloev*, 2012] and magnetopause observations from the Cluster constellation of satellites [*Escoubet et al.*, 1997] for the years 2001–2007. Below, we briefly describe these data sets.

2.1. SuperMAG Ring Current Indices

[16] SuperMAG is a collaboration of more than 350 globally distributed ground-based magnetic observatories, run by a number of national agencies [*Gjerloev*, 2009]. The SuperMAG initiative was established to provide validated data from a single source, with a common coordinate system, units, time resolution, and a coherent approach to filtering and baseline removal [*Gjerloev*, 2012].

[17] *Newell and Gjerloev* [2012] used this data set to derive a new set of magnetic indices, based on observations from 98 stations below 50° magnetic latitude with

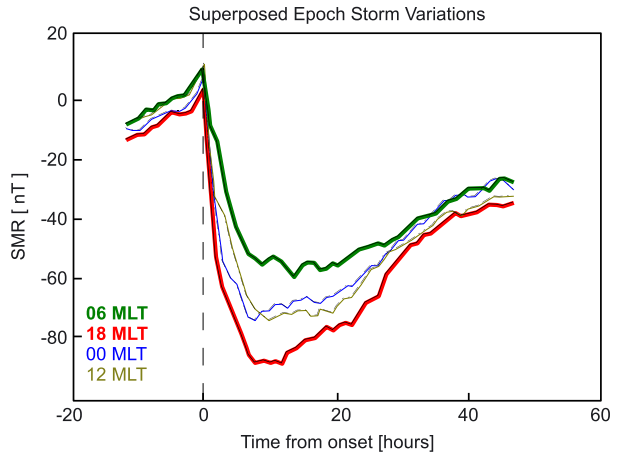

Figure 2. Superposed epoch analysis based on 125 geomagnetic storms, defined as intervals where the *Dst* index falls below –80 nT. Each color represents one of the four sectorial ring current indices. In the main phase of a geomagnetic storm, dusk perturbations (SMR18) are significantly stronger than the corresponding dawn (SMR06) perturbations. Adapted from *Newell and Gjerloev* [2012].

a dense longitudinal coverage as illustrated in Figure 1. There are some unavoidable gaps in coverage, mainly due to oceans, but the extensive longitudinal coverage allows for individual indices, designated SMR00, SMR06, SMR12 and SMR18, each providing a measure of the magnetic perturbation within their respective local time sector.

[18] The actual derivation of the sectorial indices is very similar to the method used to derive the *Dst* and SYM-H indices. A lower envelope is formed from the superposition of measurements of the horizontal magnetic field component from all stations within a local sector. The large number of stations ensures that the temporal coverage of SuperMAG indices is continuous and without data gaps, although individual contributing stations may have data gaps.

[19] This set of indices allows for a much more concise description of asymmetries in the ring current, and *Newell and Gjerloev* [2012] used the SMR indices to investigate asymmetries in the ring current during 125 identified geomagnetic storms over a 10 year period from 1997 to 2007.

[20] Figure 2 shows superposed epoch variations of the four sectorial indices for these 125 storms. This plot reveals a significant dawn-dusk asymmetry in the main phase of the storms: Magnetic perturbations on dusk, characterized by the SMR18 index, are almost twice as strong as the corresponding dawn perturbations (SMR06). Interesting is also the lack of any clear noon-midnight (SMR00 and SMR12) asymmetry. These results suggest that the ring current is significantly stronger on dusk than on dawn. As noted by *Newell and Gjerloev* [2012], the actual difference in current density may even be larger than a factor of 2, since even the observed dawnside perturbations might be influenced by the duskside ring current.

2.2. Cluster Magnetopause Observations

[21] Cluster is a four-spacecraft mission flying in a nearly 90° inclination elliptical polar orbit, with perigee around 4 R_E (even lower after 2008), apogee around 20 R_E geocentric distance, and an orbital period of approximately 57 h. During the years covered by this study, the four spacecraft were flying in close formation with separation distances varying between approximately 100 km (early 2002) up to 10,000 km (mid-2005).

[22] The instrumentation is identical on all spacecraft, but not all instruments work on all spacecraft. In the science community, the four spacecraft are referred to as SC1, SC2, SC3 and SC4, and hereafter, we use this notation to distinguish between the different spacecraft where necessary. In this study, we have used spin resolution ($\simeq$ 4 s) ion moments from the cluster ion spectroscopy/hot ion analyzer [CIS/HIA; see *Rème et al.*, 2001] and magnetic field data from the flux gate magnetometer [FGM; see *Balogh et al.*, 2001].

[23] Figure 3 shows the orbit segments relevant for our study. Cluster has its apogee near dawn during the months May, June, and July and near dusk during October to December. Due to motion of the magnetopause, each inbound or outbound traversal can consist of several crossings of the magnetopause current sheet. In particular, during late June and early July, the typical apogee is near the magnetopause boundary layer, and there are often extended

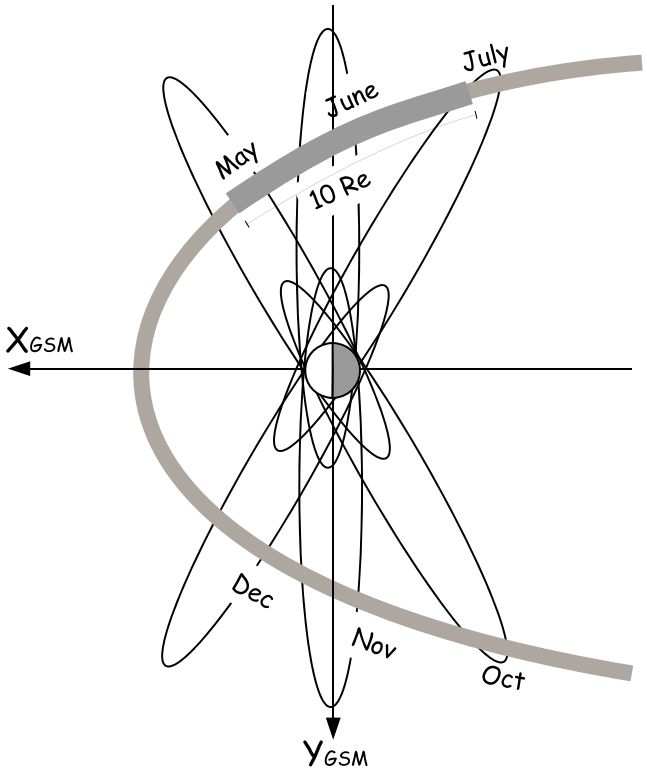

Figure 3. During May to July, and October to December, the Cluster constellation of spacecraft crosses the dawn and dusk flanks of the magnetopause, respectively. Observations from these periods are used to calculate dawn and dusk magnetopause current densities which are then compared to asymmetries in the ring current. The 10 × 10 R_E highlighted segment of the magnetopause (and a similar segment on the dusk flank) will be used to calculate total current intensity in section 3.2.

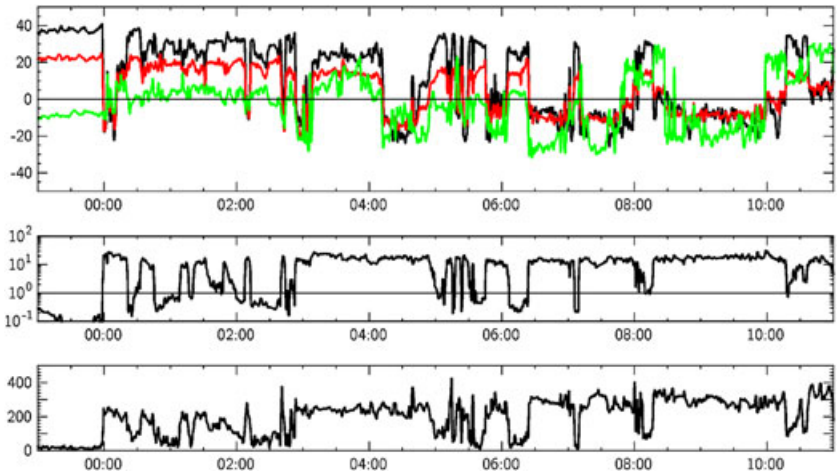

Figure 4. Example of magnetopause crossings observed by Cluster on 4–5 July 2001. (top) Magnetic field in GSE coordinates. Black, red, and green indicate the *X*, *Y*, and *Z* components, respectively. (middle) Plasma density. (bottom) Flow velocity. Due to flapping and wave motion of the magnetopause, more than 20 individual crossings can be identified in this overview. [after *Paschmann et al.*, 2005].

periods where the spacecraft constellation skims the magnetopause, resulting in a large number of crossings within one single day (Figure 4) [e.g., *Paschmann et al.*, 2005].

[24] Since most of the magnetopause traversals take place near or at Cluster apogee, our observations are typically taken close to the ecliptic plane. As explained in section 4.1, observations at high latitudes have been discarded to avoid contamination from cusp currents and effects of field-aligned currents.

2.2.1. Identifying Magnetopause Crossings

[25] To identify magnetopause crossings, we first consulted low resolution plots available from the Cluster Quick look web pages (http://www.cluster.rl.ac.uk/csdsweb-cgi/csdsweb_pick) for these periods. These interactive web pages allow users to browse the Cluster data set and plot key parameters such as spacecraft location and time series of magnetic field and plasma data. The spacecraft location plot also provides an estimated magnetopause position and estimated bow shock locations based on models.

[26] As a first criterion, we made sure that Cluster was located near the expected magnetopause position. If this criterion was fulfilled, we consulted the data plots and looked for abrupt changes in the field or plasma parameters which could indicate a transition between a fairly rigid magnetic field and low plasma density inside the magnetopause to a more turbulent magnetic field and higher plasma densities in the magnetosheath as seen in the seminal paper by *Cahill and Amazeen* [1963]. Quick look plots typically cover 6 h intervals, so an exact determination of crossing times was not possible at this stage. Due to motion of the magnetopause and surface waves, each 6 h time often contains several crossings. Times and dates for time periods where we suspected magnetopause traversals were noted.

[27] As the next step, we downloaded spin resolution magnetic field data and plasma moments from the Cluster Active Archive [*Laakso et al.*, 2010] for the times identified in the procedure above. The Quick look plots above only contain data from SC3. Since Cluster was flying in a tetrahedron-like formation, any magnetopause crossing will often (but not always) be observed by all spacecraft. Magnetic field measurements were available from all four spacecraft, but plasma moments from CIS/HIA were only available from SC1 and SC3.

[28] For each identified time period, we plotted the magnetic field, the plasma density, and plasma flow (when available) as exemplified in Figure 4. From these overview plots, we then tried to identify the magnetopause traversal times to within a minute accuracy. In this step, we also discarded partial crossings and obvious erroneous identifications (e.g., current sheets in the magnetosheath). At this stage, it often proved helpful to consult the direction of time-shifted measurements of the interplanetary magnetic field (IMF) from the Coordinated Data Analysis Web OMNI data set [see e.g., *King and Papitashvili*, 2005], where possible. In the magnetosheath, the IMF clock angle is typically not much modified [e.g., *Coleman*, 2005], and there is a close resemblance between the magnetic field direction measured by Cluster and those of the OMNI data.

[29] Events with unambiguous magnetopause signatures were kept and processed further. To obtain a more precise timing of the magnetopause crossings, and also, for the calculation of current density, we downloaded high resolution (5 vec/s) magnetic field data from the Cluster Active Archive.

[30] Figure 4 also demonstrates how dynamic the magnetopause can be. As reported in *Paschmann et al.* [2005], orientation, thickness, and velocity of the magnetopause current sheet can all vary greatly from crossing to crossing, mainly due to internal structures such as magnetic islands and undulations. Thus, simultaneous measurements from both flanks, using, e.g., Cluster observations from one flank and, e.g., the Thermal Emission Imaging System (THEMIS) spacecraft [*Angelopoulos*, 2008] at the other flank would be of limited value for a direct case-by-case dawn-dusk comparison.

3. Magnetopause Current Density

[31] We have used two different techniques to calculate the electric current density of the magnetopause. The

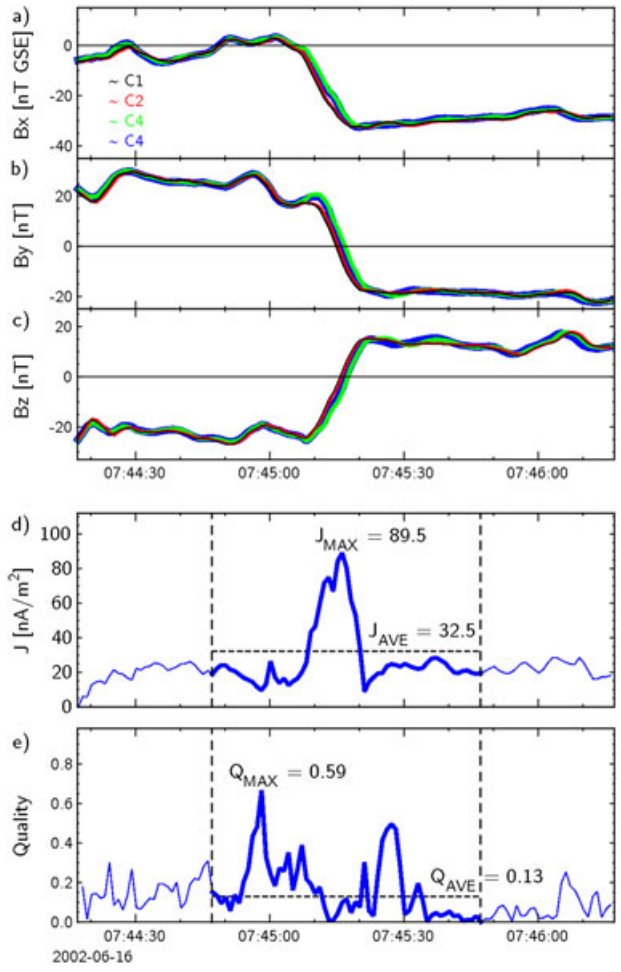

Figure 5. Example of current determination using the curlometer method. (a–c) Magnetic field components from the four Cluster spacecraft. All four spacecraft observe the field rotation nearly simultaneously, so the curves almost overlap. (d) Current density calculated from the curlometer. Vertical dashed lines indicate the 1 min time interval used to calculate the current, and the horizontal dashed line indicates the average current. (e) The ratio $Q = |\nabla \cdot \vec{B}|/(\nabla \times \vec{B})$, used a as a quality estimate. Q_{AVE}, later used for filtering, is indicated by the horizontal dashed line.

aptly named "curlometer method" requires magnetic field and position from a constellation of spacecraft, whereas the second approach—a simplified single-spacecraft method—assumes a one-dimensional magnetopause current layer and requires a combination of plasma moments and B-field to calculate the current density.

[32] The curlometer method only provides the current density, whereas the single-spacecraft method also provides the magnetopause thickness, needed to calculate the total current intensity.

3.1. Current Density From the "Curlometer" Method

[33] The curlometer method utilizes magnetic field measurements from the corners of the tetrahedron spanned by the four Cluster satellites to calculate magnetic gradients (curl and divergence). This technique has been applied to a number of Cluster studies to measure the magnetopause currents, [e.g., *Dunlop et al.*, 2002; *Dunlop and Balogh*, 2005; *Haaland et al.*, 2004; *Panov et al.*, 2006], magnetotail currents [e.g., *Shen et al.*, 2003; *Runov et al.*, 2005, 2006], and the ring current [e.g., *Vallat et al.*, 2005].

[34] Provided that the spacecraft configuration is properly formed (see e.g., *Robert et al.* [1998b, 1998a], *Chanteur* [1998], and *Chanteur and Harvey* [1998], for a discussion about this), and the spacecraft separation is small compared to the magnetopause current layer, differences in the B-field between the spacecraft can be used to estimate linear gradients. This can then be utilized to calculate the electric current density from Amperes law:

$$\mu_0 \vec{J} = \nabla \times \vec{B} \tag{1}$$

A rough estimate of the quality of the current determination is provided by the ratio

$$Q = \frac{|\nabla \cdot \vec{B}|}{\nabla \times \vec{B}} \tag{2}$$

Since a magnetic field is divergence free, Q should ideally be 0. A value close to 1 indicates that the divergence of the B-field is comparable to the curl for the event and thus not a trustworthy current density estimate. Note that the divergence of B is also based on a gradient calculation and thus is restricted by the above assumptions, so this ratio can not be used to produce an exact error estimate of the current determination.

[35] Figure 5 shows an example of Cluster measurements during a magnetopause crossing on the dawn flank on 16 June 2002. At around 07:45:10 UT, Cluster observes a strong rotation in the magnetic field (top) and a drop in plasma density (not shown) as they cross the magnetopause from the magnetosheath into the magnetosphere. The Cluster separation distance was of the order of a few hundred kilometers during this time, so all four spacecraft observe the field rotation nearly simultaneously. Application of the curlometer technique yields a peak current density of $\vec{J}_{MAX} = 89$ nAm^{-2} in the middle of the current sheet. The curl of B is always significantly larger than the divergence; $Q_{MAX} \leq 0.59$, and within the 1 min interval selected for current determination, $Q_{AVE} = 0.13$, so the result is robust.

[36] For comparison, single-spacecraft analysis, described in the next section, suggests a thickness around 600 km, a normal velocity around 43 km s^{-1}, and current densities between 88 and 98 nAm^{-2} for the four spacecraft.

[37] We routinely calculated the curlometer current for all crossings in our data set, but for a large number of cases, the spacecraft configuration is such that the results are not reliable. In particular, after 2006, the spacecraft configuration was changed so that one of the Cluster spacecraft trailed the other three with a large separation distance. Although less demanding variants of the curlometer [e.g., *Hamrin et al.*, 2008; *de Keyser et al.*, 2007; *de Keyser*, 2008] or methods using only 2 or 3 spacecraft [e.g., *Vogt et al.*, 2009] exist, much stricter assumptions are required. Our data set therefore contains curlometer calculation for the years 2001–2006 only. We have used fairly strict quality criteria when selecting events from the curlometer method and regard this method as superior to the single-spacecraft method described in next section.

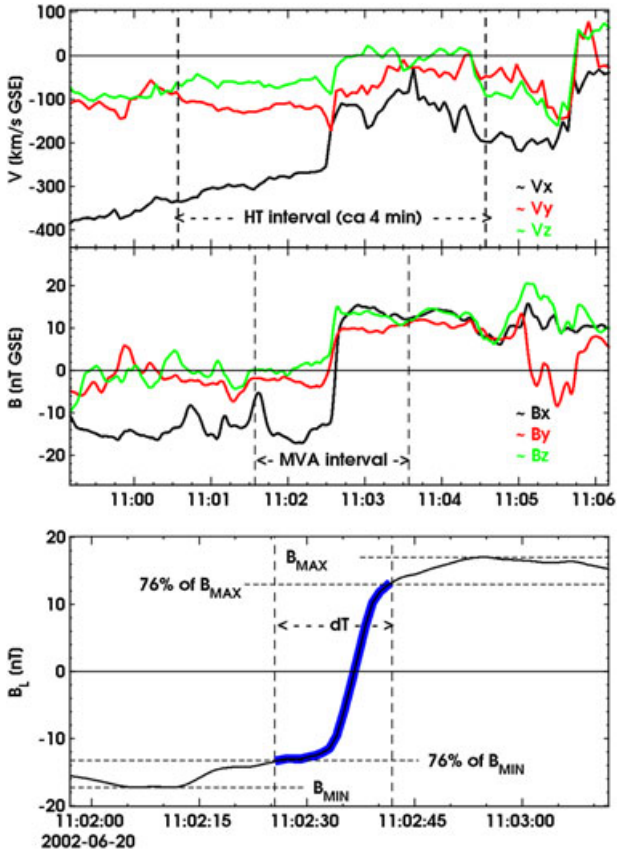

Figure 6. Example of magnetopause thickness and current calculation from single-spacecraft methods. (top) Ion velocity used to calculate magnetopause motion. (middle) Magnetic field components. (bottom) B_L (maximum variance) component of the magnetic field with the duration (dT = ΔT = time it takes to perform 76 % of the field rotation—blue part of line) indicated.

[38] The curlometer method also provides information about current direction. This will not be used in the present study, however, and when comparing currents, we use the magnitude of the curlometer current hereafter.

[39] Whereas small spacecraft separation distances are in general an advantage for the curlometer method, the often nearly simultaneous crossings of the four spacecraft combined with 0.2 s time resolution of the magnetic field also makes the determination of velocity and orientation through triangulation difficult. Magnetopause thicknesses have therefore been calculated from the single-spacecraft method.

3.2. Magnetopause Thickness and Current Density From Single-Spacecraft Observations

[40] The curlometer method fails if the magnetopause is significantly thinner than the spacecraft separation distance or if only a partial crossing takes place. For a number of events in our data set, only one, two, or three of the four Cluster spacecraft completely cross the magnetopause current layer. This is the case for the event shown in Figure 6, which shows an example of another dawnside crossing of the magnetopause, this time on 20 June 2002. Only SC1 observed a full magnetopause crossing. The spacecraft was initially in the magnetosheath, characterized by a 6–10 cm^{-3} plasma density (not shown) and high flow velocities as shown in the left part of Figure 6 (top). Around 11:02:30 UT, there is a sharp rotation in the magnetic field which indicates crossing of a thin magnetopause current sheet.

[41] For such cases, we have used a simplified approach where the local magnetopause is assumed to be a stationary, one-dimensional current sheet [*Harris*, 1962]. The current density can then be estimated from observations from a single spacecraft:

$$J = \frac{\Delta B}{\mu_0 D} = \frac{\Delta B}{\mu_0 (V_{MP} \Delta T)} \tag{3}$$

where ΔB is the jump in magnetic field magnitude across the current layer, V_{MP} is the normal velocity of the magnetopause, and ΔT is the crossing duration (see Figure 6). From the latter, the thickness $D = V_{MP} \Delta T$ can be estimated.

[42] In our study, we calculate the magnetopause orientation from a constrained minimum variance analysis of the magnetic field [MVABC; see *Sonnerup and Scheible*, 1998; *Sonnerup et al.*, 2004; *Sonnerup et al.*, 2008, for details] during a 2 min interval centered around the crossing. This minimum variance procedure provides us with a set of eigenvalues which can be used as quality criteria.

[43] As magnetopause velocity, we use the deHoffmann-Teller velocity, $\vec{V}_{HT}$ [*Khrabrov and Sonnerup*, 1998; *Paschmann and Sonnerup*, 2008] derived from ion moments and spin resolution magnetic field from Cluster SC1 and SC3. The procedure to calculate V_{HT} consists of finding a frame in which the motional electric field vanishes, $\vec{E}' = \vec{E} + \vec{V}_{HT} \times \vec{B} = 0$. In practice, this condition can not be perfectly met for all samples across the magnetopause, primarily because the stationary assumption is not satisfied. The correlation, HTcc, between the measured electric field, $\vec{E}_c = -\vec{V} \times \vec{B}$ and $\vec{E}_{HT} = -\vec{V}_{HT} \times \vec{B}$ describes how well the frame is determined and thus provides us with a quality estimate of the magnetopause velocity.

[44] For the example in Figure 6, both the magnetopause velocity and orientation of the magnetopause current sheet were well defined. For the 2 min time interval indicated in Figure 6 (middle), the minimum variance analysis had an eigenvalue ratio ($\lambda_{maximum}/\lambda_{intermediate}$) of 180. The deHoffmann-Teller frame, calculated from 4 min of plasma flow and spin magnetic field data, gave a normal velocity of approximately 24 km s^{-1} and had a correlation coefficient, HTcc = 0.93. As seen in Figure 6 (bottom), the magnetic field jump, ΔB, was approximately 34 nT, and the crossing duration was around 18 s. From equation (3), we then obtain a thickness of about 430 km and a current density of approximately 63 nAm^{-2}.

[45] Except from using a common estimate of the magnetopause velocity, we treat each spacecraft independently. During years with small spacecraft separation (e.g., during parts of 2002, the spacecraft separation were of the order of a few hundred kilometers), the calculated durations and magnetopause orientation are nearly identical between the spacecraft. For these events, there is also typically a good agreement between current densities obtained from the curlometer method and those obtained from the above single-spacecraft technique. Even with larger spacecraft

Table 1. Filter Criteria Used To Exclude Records Where Current Densities Could Not Be Accurately Determined

Quality Criteria	Method	Allowed Range	Remarks
Latitude	Both	$\leq 45°$	Avoid high-latitude or cusp crossings
Current density	"	0 to 200 nA/m^2	Remove records with unrealistic magnetopause current density
Year	Curlometer	2001–2006	Spacecraft configuration not suitable for curlometer calculations after 2006
Q_{AVE}	"	≤ 0.25	Curlometer quality estimate; see section 3.1 and equation (2)
Q_{MAX}	"	≤ 1.00	$\nabla \cdot \vec{B}$ should never exceed $\nabla \times \vec{B}$; see section 3.1 and equation (2)
MP thickness	Single SC	150 to 5000 km	Remove records with unrealistic magnetopause thickness
MVA eigenvalue ratio	"	≥ 10	Ensure well-determined determination of orientation
ΔB	"	≥ 10 nT	Make sure jump in B-field is 10 nT or more
HTcc	"	≥ 0.9	Ensure well-defined magnetopause velocity and thickness

separation distances, there is often a high degree of consistency between observations from the four spacecraft.

3.3. Total Magnetopause Current

[46] Since the above single-spacecraft method (unlike the curlometer method) also involves a step where the magnetopause thickness, D, is determined, the total current flowing through a segment of the magnetopause can be calculated:

$$I = J \times D \times L \tag{4}$$

where L is the Z_{GSM}-dimension of the magnetopause segment assumed. For simplicity, we assume that the magnetopause current near the equator flows eastward over a $Z_{GSM} = \pm 5\ R_E$ range, i.e., $L = 10\ R_E$; see Figure 3). The current density is J, which can be estimated from either of the above methods.

4. Data Set Characteristics

[47] To facilitate filtering and selection of subsets for the analysis, we stored all observations in a database. Each record in this database represents one event, i.e., one magnetopause crossing. In addition to the ring current indices and current densities from the two above methods, we also stored date and time of the event, crossing duration, Cluster position, eigenvectors and eigenvalues from the MVA analysis, magnetopause velocity, and deHoffmann-Teller correlation coefficient, as well as quality factors from the curlometer method.

[48] The full data set consists of 5483 magnetopause traversals where one or more of the Cluster satellites crosses the magnetopause crossings. In some cases, not all spacecraft crosses the magnetopause, so the total number of individual crossing observations is 16,786.

4.1. Magnetopause Data Set Quality Criteria

[49] After visual inspection of each event, we also applied a number of formal quality criteria to ensure that the key parameters such as orientation, velocity, and thickness necessary to calculate the current were correct. Records with obvious erroneous values, typically caused by data gaps or breakdown of model assumptions, were also removed. Table 1 lists the filter criteria we used to select data for analysis.

[50] Small changes in the above filter criteria do not have any significant impact on the results, though. The filter settings are quite conservative, and after having filtered the data according to these criteria, we ended up with a substantially smaller number of suitable crossings. The remaining events provide us with a subset of crossings with reliable estimates of magnetopause current densities and thicknesses, though. More importantly, there should not be any dawn-dusk bias in the data set.

[51] For 129 magnetopause crossings, all of the quality criteria in Table 1 were fulfilled, and a direct comparison between current densities from the curlometer method and the single-spacecraft method was possible. Current densities calculated with the curlometer method were on average 43% higher than those calculated with the single-spacecraft method. However, note that the curlometer method returns the peak current, whereas the single-spacecraft method returns an average over the current sheet thickness.

4.2. Ring Current Measurements

[52] SuperMAG provides a continuous monitoring of the four ring current indices, so for all of the 5483 Cluster magnetopause traversals, we have a ring current measurement from all four sectors. From these, we use a 10 min average, centered around each individual magnetopause crossing to calculate a ring current. Since many of the crossings come in sequence, sometimes with just a few seconds between the four spacecraft, there is typically significant overlap in the average interval between adjacent SMR averages during a traversal.

[53] Using the observed SMR perturbations, it is also possible to model the asymmetry in ring current intensity. For this purpose, we assume a circular ring current at a constant radial distance of 3 R_E altitude. The current intensity is modeled as a cosine, with the maximum current at dusk and minimum current at dawn.

[54] The modeling approach is a simple Biot-Savart numerical integration. First, the ring current is divided into 360 current segments. Thereafter, the magnetic field perturbation on ground produced by each individual current segment is calculated. These are then summed to produce the total perturbation. Any effects of diverging currents, e.g., field-aligned currents are ignored. By adjusting the intensity and its cosine modulation to match the observed SMR values, we thus get an idea about the magnitude of the total ring current and its azimuthal distribution.

5. Results

[55] In the following, we present the statistical results from a large number of magnetopause crossings. Due to

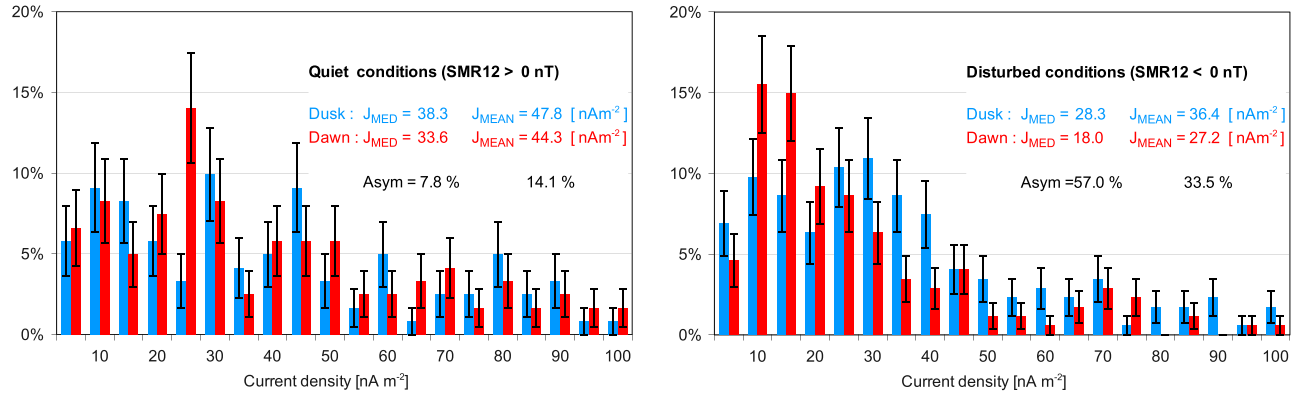

Figure 7. Distribution of magnetopause current densities based on curlometer results. Each bin in the histograms are 5 nA m^{-2} wide, and the indicated error bars are calculated as the square root of the number of observations in each bin and normalized. (left) Distribution during quiet conditions. (right) Corresponding distribution during disturbed conditions. The magnetopause current density is higher during quiet conditions, but there is a persistent dawn-dusk asymmetry in all three moments. Dusk current densities are higher, and the asymmetry is more pronounced during disturbed conditions.

the above filtering and strict quality criteria, only a part of the total data set provides reliable values. In particular, and perhaps somewhat surprising is the fact that reasonable curlometer results could only be obtained from less than 20% of the magnetopause crossings. A more relaxed set of quality criteria would certainly have provided a larger number of events but probably at the cost of robustness of the results.

[56] For convenience, we simply use the SMR12 index, readily available from our data set, as a proxy for disturbance level. Using, e.g., SMR00 or an average of the four sectorial indices leads to small shifts in the numbers but does not alter the outcome of the study.

[57] Only a handful of Cluster magnetopause crossings happens to take place during the main phase of a geomagnetic storm, and the *Dst* (SMR12) range of our filtered data set (i.e., where reliable magnetopause current density estimates are available) is limited to values between –80 and + 40 nT, with rather few observations for the extremes. We are thus not able to derive any meaningful results for all phases of a geomagnetic storms or provide a correlation coefficient between SMR and magnetopause dawn-dusk asymmetry. In the discussion below, we refer to SMR12 values of 0 nT and higher as quiet conditions and SMR12 values below 0 nT as disturbed.

[58] To characterize the data, we use the three main statistical moments: mean, median, and mode. We also provide the standard error (StdErr—defined as the standard deviation divided by the square root of the number of observations) as a measure of spread in the data. Whereas the mean and median moments are straightforward and unique for a given distribution, one should keep in mind that the mode (most frequent value within a distribution) is not always unique and also depends on the binning.

5.1. Dawn and Dusk Magnetopause Current Densities

[59] Figure 7 shows the normalized distribution of the magnetopause currents for quiet (left) and disturbed (right) geomagnetic conditions. Each bin in these histograms is 5 nA/m^2 wide, and the indicated error bars are calculated as the square root of the number of observations in each bin and normalized. Red bars indicate dawn current densities; blue bars show dusk current densities.

[60] For quiet conditions, the dawn mode is 20–25 nA m^{-2}, whereas the corresponding dusk mode current density is 25–30 nA m^{-2}. Mean and median current density values are also larger on the duskside. The asymmetry, here defined as follows:

$$A = \frac{J_{\mathrm{DUSK}} - J_{\mathrm{DAWN}}}{J_{\mathrm{DAWN}}} \tag{5}$$

is 7.8% for the mean current density and 14.1% for the median current density.

[61] For disturbed conditions, i.e., SMR12 values below 0 nT, the dawn mode current is 5–10 nA m^{-2}, whereas the corresponding dusk mode is now 25–30 nA m^{-2}. Dawn-dusk asymmetries in mean and median current densities are now larger; median and mean dusk currents are 33% and 57% larger than their dawn counterparts, respectively. The asymmetry becomes even more pronounced if we select more disturbed conditions. For SMR12 values below –20 nT, the dusk current densities are 63% (median) and 33% (mean) larger than dawn current densities.

[62] The current densities thus seem to follow the trend seen in the SMR indices. Dusk magnetopause current densities are generally larger, and the asymmetry between dawn and dusk increases with disturbance level.

[63] The fact that magnetopause current densities seem to be larger during quiet conditions may seem contradictory. However, recall that magnetopause currents must provide the $\vec{J} \times \vec{B}$ force to balance the rate of change of solar wind momentum, $\rho \vec{V}_{\mathrm{SW}}^{2}$. The strength of the magnetopause current is primarily governed by the solar wind pressure [e.g., *Burton et al.*, 1975; *van Allen and Adnan*, 1992; *O'Brien and McPherron*, 2000], and positive *Dst* values (or equivalent, our SMR12 proxy) are often associated with high solar wind pressure. This is corroborated by the magnetopause thickness values; during quiet times, both dawn and dusk are thinner than during disturbed conditions.

Table 2. Data Set Characteristics[a]

Disturbance Level (SMR12)[b]		Ring Current: SMR Indices [nT][c] SMR06 (Dawn)	Ring Current: SMR Indices [nT][c] SMR18 (Dusk)	Ring Current: Total Current [10^6A][d] Dawn	Ring Current: Total Current [10^6A][d] Dusk	Magnetopause: Current Density [nA m^{-2}][e] Dawn	Magnetopause: Current Density [nA m^{-2}][e] Dusk	Magnetopause: Thickness (km)[f] Dawn	Magnetopause: Thickness (km)[f] Dusk	Magnetopause: Total Current [10^6A] (Equation (4))[g] Dawn	Magnetopause: Total Current [10^6A] (Equation (4))[g] Dusk
	Num. obs	5483	5483			328	463	1112	969	1112	969
All	Mean	-3.9	**-7.9**	0.00	0.33	37.4	**38.5**	**1810**	1499	**4.44**	3.68
	Median	-2.5	**-3.6**	0.05	0.12	24.5	**29.0**	**1501**	1063	**2.22**	1.97
	StdErr	0.2	0.3			1.9	1.4	1258	1190	0.08	0.07
	Num. obs	2296	2296			121	124	456	390	121	124
Quiet:	Mean	**6.1**	6.4	–0.16	–0.19	**47.8**	44.3	**1715**	1487	**4.84**	4.53
SMR12	Median	**3.8**	4.7	–0.09	–0.15	**38.3**	33.6	**1393**	887	**2.98**	2.17
$\geq$ 0 nT	StdErr	0.2	0.2			3.5	3.3	1242	1204	0.27	0.26
	Num. obs	3187	3187			144	174	656	579	144	174
Disturbed:	Mean	-11.1	**-18.2**	0.09	0.73	27.2	**36.4**	**1874**	1507	3.25	**3.49**
SMR12	Median	-7.9	**-9.9**	0.16	0.34	18.0	**28.2**	**1572**	1163	1.81	**2.10**
< 0 nT	StdErr	0.3	0.5			2.2	2.3	1266	1181	0.18	0.17

[a]Highlighted text indicate the largest (absolute) observed value in each sector. Overall, the SMR perturbations are larger on dusk and become larger during disturbed conditions. The magnetopause current densities derived from the curlometer method are also consistently larger on the dusk. On the other hand, the magnetopause seems to be thicker on the dawn flank. The various columns indicate

[b]We use the SMR12 index as a proxy for disturbance level.

[c]Num. obs = number of observations. SMR values are always available, so data from all 5483 crossings can be used.

[d]Model calculations; see section 5.2 for details.

[e]Current densities from the curlometer method.

[f]Magnetopause thickness, estimated from the duration of the crossing; see Figure 6.

[g]Total magnetopause current flowing through a 10 R_E long section; see equation (4).

5.2. Ring Current Versus Magnetopause Currents

[64] Table 2 shows detailed characteristics of the full data set as well as the two subsets with quiet and disturbed conditions, respectively. In column D, we also show the modeled ring current (see section 4.2 for details) to give an idea about the current intensity required to produce the observed SMR values.

[65] For quiet conditions, the average SMR06 and SMR18 indices are both positive, indicating that the ground magnetic perturbations are dominated by the inner, eastward component of the ring current [*Jorgensen et al.*, 2004; *Le et al.*, 2004]. In our simplified ring current model with a single-line current at 3 R_E radial distance; however, positive SMR values imply a net eastward ring current—thus the minus sign for total current.

[66] Overall, the SMR perturbations are larger on the duskside. The dawn-dusk differences become more pronounced during disturbed conditions—in agreement with the *Newell and Gjerloev* [2012] results. Magnetopause current densities as obtained from the curlometer method current also show the same behavior; except for quiet conditions (positive SMR12 values), magnetopause current densities are consistently higher on the duskside. The dawn-dusk asymmetry in the magnetopause current is larger for disturbed conditions than for quiet or moderate disturbance levels—also consistent with the ring current behavior.

5.3. Error Sources in the Results

[67] While we believe that the dawn-dusk asymmetries are significant and real, a few words about the credibility of the results may be in its place before we start discussing implications of the above findings. As with any collection of experimental data, there are uncertainties related to both measurements, methodology, and the underlying assumptions. Below, we try assess the effect of each of these factors.

[68] **Measurement Errors:** Measurements from the Cluster FGM and CIS/HIA instruments are accurate and well calibrated. Regular cross-calibration efforts, both in the form of intercalibration between the four spacecraft and also by cross checks against other instruments, are performed regularly [*Laakso et al.*, 2010]. The same applies to measurements from the ground magnetic observations used to derive the SMR indices. Each sectorial SMR index is based on 5 to 20 ground stations, and local time gradients at ring current latitudes are smaller than in, e.g., the auroral zone. Thus, our assessment is that individual measurement errors are small and should not introduce any dawn-dusk asymmetry neither in the ring current estimation nor in the magnetopause measurements.

[69] **Model Assumptions and Methodology:** To calculate magnetopause current densities, we make assumptions about the geometry and stationarity of the magnetopause. For the single-spacecraft technique, methods to estimate errors exist for both the minimum variance analysis [see, e.g., *Sonnerup et al.*, 2008] and for the deHoffmann-Teller velocity estimations [e.g., *Paschmann and Sonnerup*, 2008]. These error analyses can only account for statistical errors from the minimization schemes involved in both methods. The strict filter criteria used ensure that these statistical errors are small. Actual errors can be much larger, primarily as a consequence of violations of the underlying assumptions. In reality, the magnetopause is rarely stationary nor one-dimensional. Whereas observations of persistent dawn-dusk asymmetries in magnetosheath properties exist [e.g., *Wing et al.*, 2005; *Longmore et al.*, 2005], it is unclear whether this or any other effects introduce any significant dawn-dusk bias in the magnetopause model assumptions.

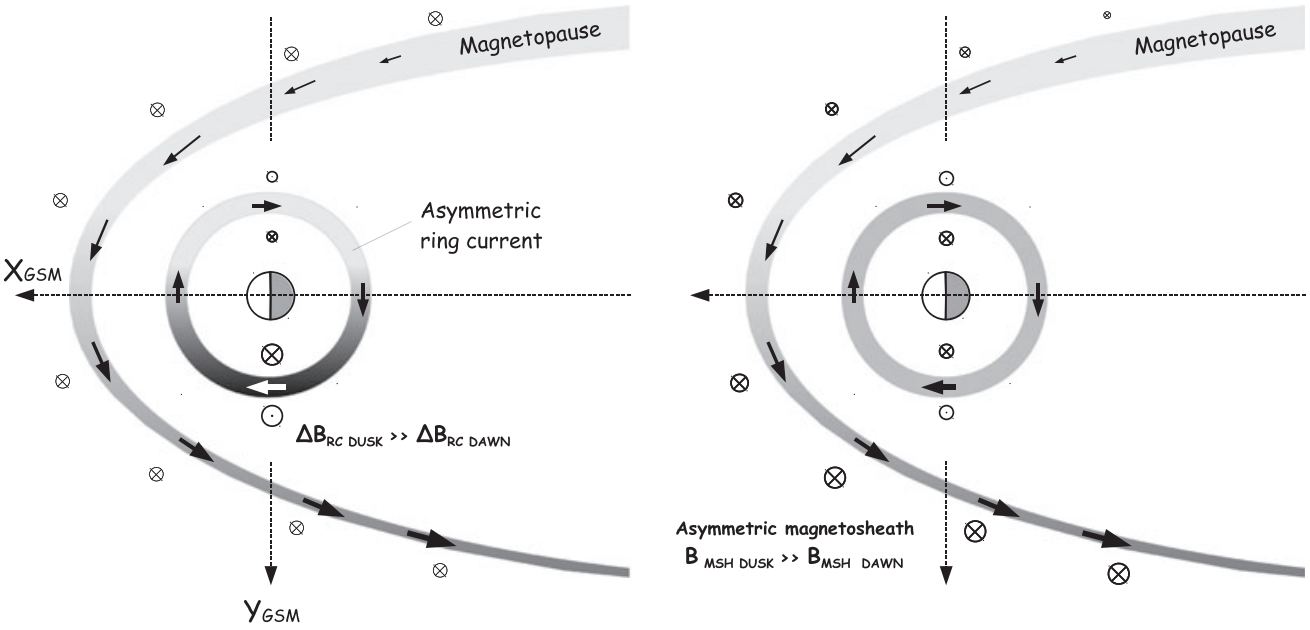

Figure 8. Illustration of possible explanations for the observed dawn-dusk magnetopause asymmetry. Light shading indicates low current density; darker shadings indicate higher current densities. Arrows indicate current direction and strength. (left) Asymmetries caused by ring current. Since the ring current is more intense in the dusk sector, magnetic field perturbations are larger on dusk. Assuming a symmetric magnetosheath field, this leads to a higher magnetic shear and consequently higher current density at the dusk magnetopause. (right) Asymmetries caused by asymmetric magnetosheath conditions. Even for a symmetric ring current, differences in magnetic field and/or dynamic pressure in the magnetosheath can lead to a higher magnetic shear and thus a higher current density at the duskside magnetopause.

[70] **External Influences:** Our data set also contains measurements of the interplanetary magnetic field (IMF). Interactions between the Parker spiral-like interplanetary magnetic field with the Earth's bow shock are known to introduce dawn-dusk asymmetries [e.g., *Walsh et al.*, 2012]. In our data set, IMF By values are not very different for the dawn and dusk data set; for the full data set in Table 2, the average IMF By during dawn and dusk crossings are 0.6 nT and 1.1 nT, respectively, so there should not be any significant dawn-dusk asymmetries due to bias in the IMF conditions. The Parker spiral-like configuration of the IMF or the solar wind aberration can not fully explain the observed asymmetry.

[71] **Statistical Spread:** As seen in Table 2, there is quite a lot of spread in both SMR indices and currents. Note that these spreads mainly reflect the genuine variability in both the ring current and the magnetopause—the calculated standard errors should not be interpreted as errors in measurements or methodology. From Table 2, we note that the statistical spreads on dawn and dusk are comparable for the magnetopause parameters. The dusk ring current (reflected by SMR18) seems to possess somewhat higher variability than its dawn counterpart.

6. Discussion

[72] In summary, the ring current and magnetopause current show a similar behavior when it comes to dawn-dusk asymmetry. The response to geomagnetic activity is also similar for the two current systems.

[73] From the above consistencies, one might be tempted to conclude that there must be a connection between the ring current and the magnetopause in the form of a current loop. However, the thickness calculations, albeit based on slightly less accurate single-spacecraft methods, indicate that the dawn magnetopause current layer is thicker than the corresponding dusk layer. This is in itself an interesting result, and to our knowledge, this has not been studied with such an extensive data set earlier.

[74] The findings nevertheless suggest a mutual coupling between the two current systems, but the cause and effect is difficult to assess: Magnetic perturbations caused by the ring current can influence the magnetic shear at the magnetopause. But the vice versa is also true: Magnetopause currents can contribute to observed ground-based observations.

6.1. Ring Current Influence on the Magnetopause

[75] To illustrate how the ring current can influence the magnetopause current density, consider Figure 8 (left), which illustrates the ring current and the magnetopause current in the equatorial plane. For simplicity, we will assume that the magnetosheath properties on the two flanks are identical, and that the ring current can be modeled by a line current at a fixed radial distance from the Earth. Also, we ignore any ring current closure issues for the moment and simply consider the observed fact that the ring current is more intense in the dusk sector.

[76] Under these assumptions, magnetic perturbation from the ring current will be larger on the duskside, thus

leading to a higher magnetic shear near the dusk magnetopause. From Ampère's law, a higher magnetic shear translates into a higher current density—consistent with the Cluster observations. If we assume that the magnetopause current is entirely a Chapman-Ferraro current, the number of charge carriers will be the same on dawn and dusk. The only way to obtain a higher duskside magnetopause current density is thus to reduce the thickness of the magnetopause current layer—this is indeed what the Cluster observations show.

6.2. Contribution to SMR From the Magnetopause

[77] Measured perturbations of the magnetic field at the surface of the Earth, as reflected by the SMR indices, are the result of a collective effect of a number of current systems. The symmetric ring current and the partial ring current are the dominant contributors, but also, tail currents and magnetopause currents contribute.

[78] Dawn-dusk asymmetries in the magnetopause can also arise as a consequence of asymmetries in the magnetosheath. *Walsh et al.* [2012] recently reported observations from the THEMIS spacecraft which showed a dawn-dusk asymmetry in plasma and field parameters in the Earth's magnetosheath. Proton density and temperature were greater on the dawnside, while the magnetic field strength and bulk flow were greater on the duskside. The asymmetries were attributed to the geometry of the bow shock. Other studies [e.g., *Wing et al.*, 2005] suggested that magnetosheath asymmetries are primarily a result of gradient drift in the magnetosphere. Using the same arguments as in the previous section, the larger magnetic shear on the duskside implies a higher current density on the duskside.

[79] Not only the strength of magnetopause currents but also their distance from the Earth's surface plays a role, and the effect on ground magnetic perturbations is larger near the dayside where the magnetopause is closer to Earth. *Burton et al.* [1975] derived an empirical relationship between interplanetary conditions and *Dst*. They noted that the contribution to *Dst* during storm time conditions could be expressed as $Dst_{\mathrm{MP}} = 15.5 \times \sqrt{P_{\mathrm{DYN}}}$, where P_{DYN} is the solar wind dynamic pressure. A later study by *O'Brien and McPherron* [2000] suggested a lower magnetopause contribution: $Dst_{\mathrm{MPs}} = 7.2 \times \sqrt{P_{\mathrm{DYN}}}$. Our magnetopause data set from Cluster presently does not contain solar wind dynamic pressure measurements, so it is not possible to quantify magnetopause contributions to the SMR values.

7. Summary

[80] We have investigated the connection between asymmetries in the ring current and magnetopause currents. Based on a total of 5843 observations where one or more Cluster spacecraft cross the magnetopause, we calculated the orientation, thickness, and current density of the magnetopause current layer. For a number of cases, the spacecraft configuration also allowed current determination using the four-spacecraft curlometer method.

[81] The results can be summarized as follows:

[82] 1. The ring current measurements in our data set suggest a persistent dawn-dusk asymmetry with stronger ground magnetic perturbations in the dusk sector. We interpret this as the result of a more intense ring current in the dusk sector.

[83] 2. The ring current dawn-dusk asymmetry becomes stronger during disturbed geomagnetic conditions. A similar development is seen in the magnetopause current density.

[84] 3. Duskside magnetopause current densities are persistently stronger than their dawnside counterparts. We primarily attribute this to enhanced magnetic shear caused by a stronger dusk ring current, though asymmetries in the magnetosheath may also contribute.

[85] 4. The dawn magnetopause is thicker than the dusk magnetopause.

[86] 5. We have not been able to unambiguously identify a direct connection in the form of a current loop between the ring current and magnetopause current, but the consistency in behavior of the two current systems does not exclude such a loop, however.

[87] **Acknowledgments.** SuperMAG is funded by NSF grant 1003580 and ESA PRODEX contract 4000104152. Computer code used for the calculations in this paper has been made available as part of the QSAS science analysis system. QSAS is provided by the United Kingdom Cluster Science Centre (Imperial College London and Queen Mary, University of London) supported by the United Kingdom Science and Technology Facilities Council (STFC). Solar wind data were obtained from the Coordinated Data Analysis Web (CDAWeb - see http://cdaweb.gsfc.nasa.gov/about.html). We thank Chandrasekhar Anekallu and Stephen Fuselier for valuable discussions. We also thank the International Space Science Institute, Bern, Switzerland for providing computer resources and infrastructure for data exchange.

[88] Masaki Fujimoto thanks Johan DeKeyser and Amy Keesee for their assistance in evaluating this paper.

References

Akasofu, S.-I. (1980), The solar wind-magnetosphere energy coupling and magnetospheric disturbances, *Planet. Space Sci.*, *28*, 495–509.

Akasofu, S.-I., and S. Chapman (1961), The ring current, geomagnetic disturbance, and the Van Allen radiation belts, *J. Geophys. Res.*, *66*, 1321–1350.

Akasofu, S.-I., and S. Chapman (1964), On the asymmetric development of magnetic storm fields in low and middle latitudes, *Planet. Space Sci.*, *12*, 607.

Angelopoulos, V. (2008),The THEMIS mission, *Space Sci. Rev.*, *141*,5–34.

Balogh, A., et al. (2001), The cluster magnetic field investigation: Overview of in-flight performance and initial results, *Ann. Geophys.*, *19*, 1207–1217.

Burton, R. K., R. L. McPherron, and C. T. Russell (1975), An empirical relationship between interplanetary conditions and Dst, *J. Geophys. Res.*, *80*, 4204–4214.

Cahill, L. J., and P. G. Amazeen (1963), The boundary of the geomagnetic field, *J. Geophys. Res.*, *68*, 1835–1843.

Chanteur, G. (1998), Spatial interpolation for four spacecraft: Theory, *ISSI Sci. Rep. Ser.*, *1*, 349–370.

Chanteur, G., and C. C. Harvey (1998), Spatial interpolation for four spacecraft: Application to magnetic gradients, *ISSI Sci. Rep. Ser.*, *1*, 371–394.

Chapman, S., and V. C. A. Ferraro (1930), A new theory of magnetic storms, *Nature*, *126*, 129–130.

Coleman, I. J. (2005), A multi-spacecraft survey of magnetic field line draping in the dayside magnetosheath, *Ann. Geophys.*, *23*, 885–900.

Crooker, N. U. (1972), High-time resolution of the low-latitude asymmetric disturbance in the geomagnetic field, *J. Geophys. Res.*, *77*, 773–775.

Crooker, N. U., and R. L. McPherron (1972), On the distinction between the auroral electrojet and partial ring current systems, *J. Geophys. Res.*, *77*, 6886.

Cummings, W. D. (1966), Asymmetric ring currents and the low-latitude disturbance daily variation, *J. Geophys. Res.*, *71*, 4495–4503.

de Keyser, J. (2008), Least-squares multi-spacecraft gradient calculation with automatic error estimation, *Ann. Geophys.*, *26*, 3295–3316.

de Keyser, J., F. Darrouzet, and M. W. Dunlop (2007), Least-squares gradient calculation from multi-point observations of scalar and vector fields: Methodology and applications with Cluster in the plasmasphere, *Ann. Geophys.*, *25*, 971–987.

Dunlop, M. W., and A. Balogh (2005), Magnetopause current as seen by Cluster, *Ann. Geophys.*, *23*, 901–907.

Dunlop, M. W., A. Balogh, K.-H. Glassmeier, and P. Robert (2002), Four-point cluster application of magnetic field analysis tools: The curlometer, *J. Geophys. Res.*, *107*, 1384, doi:10.1029/2001JA005088.

Egeland, A., and W. J. Burke (2012), The ring current: A short biography, *Hist. Geo Space Sci.*, *3*, 131–142.

Escoubet, C. P., R. Schmidt, and M. L. Goldstein (1997), Cluster - science and mission overview, *Space Sci. Rev.*, *79*, 11–32.

Frank, L. A. (1970), Direct detection of asymmetric increases of extraterrestrial ring current: Proton intensities in the outer radiation zone, *J. Geophys. Res.*, *75*, 1263.

Fukushima, N., and Y. Kamide (1973), Contribution of magnetospheric field-aligned current to geomagnetic bays and Sq fields: A comment on partial ring-current models, *Radio Sci.*, *8*, 1013.

Gjerloev, J. W. (2009), A global ground-based magnetometer initiative, *EOS Transactions*, *90*, 230–231.

Gjerloev, J. W (2012), The SuperMAG data processing technique, *J. Geophys. Res.*, *117*, 9213, doi:10.1029/2012JA017683.

Haaland, S., B. U. Ö. Sonnerup, M. W. Dunlop, A. Balogh, H. Hasegawa, B. Klecker, G. Paschmann, B. Lavraud, I. Dandouras, and H. Rème (2004), Four-spacecraft determination of magnetopause orientation, motion and thickness: Comparison with results from single-spacecraft methods, *Ann. Geophys.*, *22*, 1.

Hamrin, M., K. Rönnmark, N. Börlin, J. Vedin, and A. Vaivads (2008), GALS—Gradient Analysis by Least Squares, *Ann. Geophys.*, *26*, 3491–3499.

Harris, E. G. (1962), On the plasma sheath separating regions of oppositely directed magnetic field, *Nuovo Cimento*, *23*, 115–121.

Hasegawa, H. (2012), Structure and dynamics of the magnetopause and its boundary layers, *Monographs on Environment, Earth and Planets*, *1*, 71–119.

Iijima, T., T. A. Potemra, and L. J. Zanetti (1990), Large-scale characteristics of magnetospheric equatorial currents, *J. Geophys. Res.*, *95*, 991–999.

Jorgensen, A. M., H. E. Spence, W. J. Hughes, and H. J. Singer (2004), A statistical study of the global structure of the ring current, *109*, 12,204.

Kawasaki, K., and S.-I. Akasofu (1971), Geomagnetic storm fields near a synchronous satellite, *Planet. Space Sci.*, *19*, 1339–1347.

Khrabrov, A. V., and B. U. Ö Sonnerup (1998), Orientation and motion of current layers: Minimization of the Faraday residue, *Geophys. Res. Lett.*, *25*, 2373.

King, J. H., and N. E. Papitashvili (2005), Solar wind spatial scales in and comparisons of hourly Wind and ACE plasma and magnetic field data, *J. Geophys. Res.*, *110*, 2104, doi:10.1029/2004JA010649.

Laakso, H., M. Taylor, and C. P. Escoubet (2010), *The Cluster Active Archive*, Springer, Noordwiijk, Netherlands.

Langel, R. A., and R. E. Sweeney (1971), Asymmetric ring current at twilight local time, *J. Geophys. Res.*, *76*, 4420–4427.

Le, G., C. Russell, and K. Takahashi (2004), Morphology of the ring current derived from magnetic field observations, *Ann. Geophys.*, *22*, 1267–1295.

Liemohn, M. W., J. U. Kozyra, M. F. Thomsen, J. L. Roeder, G. Lu, J. E. Borovsky, and T. E. Cayton (2001), Dominant role of the asymmetric ring current in producing the stormtime Dst*, *J. Geophys. Res.*, *106*, 10,883–10,904.

Liu, S., M. W. Chen, M. Schulz, and L. R. Lyons (2006), Initial simulation results of storm-time ring current in a self-consistent magnetic field model, *J. Geophys. Res.*, *111*, 4225, doi:10.1029/2005JA011194.

Longmore, M., S. J. Schwartz, J. Geach, B. M. A. Cooling, I. Dandouras, E. A. Lucek, and A. N. Fazakerley (2005), Dawn-dusk asymmetries and sub-Alfvénic flow in the high and low latitude magnetosheath, *Ann. Geophys.*, *23*, 3351–3364.

Newell, P. T., and J. W. Gjerloev (2012), SuperMAG-based partial ring current indices, *J. Geophys. Res.*, *117*, 5215, doi:10.1029/2012JA017586.

O'Brien, T. P., and R. L. McPherron (2000), An empirical phase space analysis of ring current dynamics: Solar wind control of injection and decay, *J. Geophys. Res.*, *105*, 7707–7720.

Panov, E. V., J. Büchner, M. Franz, A. Korth, Y. Khotyaintsev, B. Nikutowski, S. Savin, K.-H. Fornaçon, I. Dandouras, and H. Rème (2006), CLUSTER spacecraft observation of a thin current sheet at the Earth's magnetopause, *Adv. Space Res.*, *37*, 1363–1372.

Paschmann, G., and B. U. Ö. Sonnerup (2008), Proper frame determination and Walen test, *ISSI Sci. Rep. Ser.*, *8*, 65–74.

Paschmann, G., S. Haaland, B. U. Ö. Sonnerup, H. Hasegawa, E. Georgescu, B. Klecker, T. D. Phan, H. Rème, and A. Vaivads (2005), Characteristics of the near-tail dawn magnetopause and boundary layer, *Ann. Geophys.*, *23*, 1481.

Rème, H., et al. (2001), First multispacecraft ion measurements in and near the Earth's magnetosphere with the identical Cluster ion spectrometry (CIS) experiment, *Ann. Geophys.*, *19*, 1303–1354.

Robert, P., M. W. Dunlop, A. Roux, and G. Chanteur (1998a), Accuracy of current density determination, *ISSI Sci. Rep. Ser.*, *1*, 395–418.

Robert, P., A. Roux, C. C. Harvey, M. W. Dunlop, P. W. Daly, and K.-H. Glassmeier (1998b), Tetrahedron geometric factors, *ISSI Sci. Rep. Ser.*, *1*, 323–348.

Runov, A., V. A. Sergeev, R. Nakamura, W. Baumjohann, T. L. Zhang, Y. Asano, M. Volwerk, Z. Vörös, A. Balogh, and H. Rème (2005), Reconstruction of the magnetotail current sheet structure using multi-point Cluster measurements, *Planet. Space Sci.*, *53*, 237–243.

Runov, A., et al. (2006), Local structure of the magnetotail current sheet: 2001 Cluster observations, *Ann. Geophys.*, *24*, 247–262.

Shen, C., X. Li, M. Dunlop, Z. X. Liu, A. Balogh, D. N. Baker, M. Hapgood, and X. Wang (2003), Analyses on the geometrical structure of magnetic field in the current sheet based on cluster measurements, *J. Geophys. Res.*, *108*, 1168, doi:10.1029/2002JA009612.

Smith, E. J., P. J. Coleman Jr., D. L. Judge, and C. P. Sonett (1960), Characteristics of the extraterrestrial current system: Explorer VI and Pioneer V, *J. Geophys. Res.*, *65*, 1858.

Sonnerup, B. U., S. E. Haaland, and G. Paschmann (2008), Discontinuity orientation, motion, and thickness, *ISSI Sci. Rep. Ser.*, *8*, 1–16.

Sonnerup, B. U. Ö., and M. Scheible (1998), Minimum and maximum variance analysis, in *Analysis Methods for Multi-Spacecraft Data,* ISSI SR-001, edited by G. Paschmann and P. W. Daly, pp. 1850, ESA Publications Division, Noordwiijk, Netherlands.

Sonnerup, B. U. Ö., S. Haaland, G. Paschmann, B. Lavraud, and M. Dunlop (2004), Orientation and motion of a discontinuity from single-spacecraft measurements of plasma velocity and density: Minimum massflux residue, *J. Geophys. Res.*, *109*, A03221, doi:10.1029/2003JA010230.

Størmer, C. (1912), Sur les trajectories des corpuscules délectrisités dans l'espace sous l'actions du magnétisme terrestre avec application aux aurores boréales, *Arch. Sci.Phys. Nat.*, *33*, 51–69 and 113–150.

Vallat, C., I. Dandouras, M. Dunlop, A. Balogh, E. Lucek, G. K. Parks, M. Wilber, E. C. Roelof, G. Chanteur, and H. Rème (2005), First current density measurements in the ring current region using simultaneous multi-spacecraft CLUSTER-FGM data, *Ann. Geophys.*, *23*, 1849–1865.

van Allen, J. A., and J. Adnan (1992), Observed currents on the Earth's high-latitude magnetopause, *J. Geophys. Res.*, *97*, 6381–6395.

Vogt, J., A. Albert, and O. Marghitu (2009), Analysis of three-spacecraft data using planar reciprocal vectors: Methodological framework and spatial gradient estimation, *AAnn. Geophys.*, *27*, 3249–3273.

Walsh, B. M., D. G. Sibeck, Y. Wang, and D. H. Fairfield (2012), Dawn-dusk asymmetries in the Earth's magnetosheath, *J. Geophys. Res.*, *117*, 12,211, doi:10.1029/2012JA018240.

Weygand, J. M., and R. L. McPherron (2006), Dependence of ring current asymmetry on storm phase, *J. Geophys. Res.*, *111*, 11,221, doi:10.1029/2006JA011808.

Wing, S., J. R. Johnson, P. T. Newell, and C.-I. Meng (2005), Dawn-dusk asymmetries, ion spectra, and sources in the northward interplanetary magnetic field plasma sheet, *J. Geophys. Res.*, *110*, 8205, doi:10.1029/2005JA011086.